N95-14672

Propagation Characteristics of 20/30 GHz Links with a 40° Masking Angle

F. Davarian, A. Kantak, And C. Le
Jet Propulsion Laboratory
California Institute of Technology

1. Introduction

Because of a great demand for wireless communications, the available spectrum at frequencies lower than 18 GHz cannot meet the rapidly growing needs of the satellite communications industry. In contrast, K_a-band frequencies, which span from about 18 to over 30 GHz, offer large segments of the radio spectrum for satellite communication applications. The International Telecommunications Union (ITU) spectrum allocation for satellite communications at the K_a-band exceeds 3 GHz in each direction and currently is underutilized.

The scarcity of bands below about 18 GHz coincides with an explosive increase in demand for wireless communication services in the U.S. and elsewhere during the 1990s. Hence, spectrum shortage can severely impede industrial development as well as growth in certain sectors of the economy. Therefore, the recent interest in K_a-band frequencies for Earth/space communications is expected and should be encouraged.

On the negative side, atmospheric effects are considerably higher at K_a-band than at frequencies below about 18 GHz. It is therefore recognized that frequencies above about 18 GHz cannot be successfully exploited unless the atmospheric-induced anomalies are understood, accounted for, and mitigated. For over two decades, the United States' NASA Propagation Program and other investigators abroad have studied K_a-band propagation to improve our knowledge of the field and to find means of enhancing channel availability. These investigations have been fruitful, producing data and models that can be used for Earth/space propagation effects prediction.

An effective means of reducing K_a-band propagation loss is the use of high elevation angle paths, i.e., a large masking angle, between Earth stations and the space platform. Experimental data have shown that the signal loss associated with most atmospheric effects is inversely proportional to $\sin(\theta)$, where θ denotes the path elevation angle. A large masking angle and a

generous link margin are the primary tools used in the Teledesic Corporation network to minimize atmospheric-related signal outages. This report documents the results of a study sponsored by Teledesic Corporation to characterize the effect of radiowave propagation on Teledesic's links.

CCIR recommendations and NASA Propagation Handbooks are the main sources of propagation data and models [1,2]. The recent Olympus campaign in Europe and the U.S. has provided new information that is not included in these sources yet. Therefore, CCIR recommendations and NASA Propagation Handbook models constitute the base of this study, and, when applicable, data from other sources have been used to improve the predictions. Furthermore, attention has been given to data from the Olympus campaign.

The effects investigated during this study include gas, rain, fog, sand, and cloud attenuation, diversity gain, scintillation, and depolarization.

2. Gaseous Attenuation

Although gaseous absorption for frequencies below about 18 GHz may be ignored for most applications, K_a-band atmospheric attenuation may exceed 1 dB for small percentages of the time. Gaseous absorption is mainly due to oxygen and water vapor in the atmosphere. Oxygen produces a small but constant loss, whereas water vapor attenuation demonstrates diurnal and seasonal variations that can become much larger than the oxygen contribution.

Oxygen attenuation gradually increases by frequency, greater for 30 GHz than 20 GHz. Water vapor attenuation peaks around 22 GHz, and it is less at 30 GHz than 20 GHz. Since water vapor attenuation is proportional to water density in the atmosphere, large values of attenuation occur during warm and humid days.

Both the oxygen and water vapor effects can be estimated by a CCIR recommendation on this subject. The procedure involves the calculation of the specific attentions in dB/km and scale heights in km. The scale height used in calculating the water vapor effect is less for no-rain periods than rainy periods. Figure 1 shows the atmospheric K_a-band attenuation as a function of relative humidity at surface temperatures of 20° C and 30° C, assuming site location at sea level and no rain. Gaseous attenuation during rain is shown in Figure 2 for temperatures of 20° C and 30° C. Both figures use a path elevation angle of 40°.

For dry regions of the Earth, i.e., where relative humidity is about 20% at a temperature of 20° C, it appears that a gaseous attenuation margin of 0.3 dB is adequate. For warm and humid regions, i.e., where relative humidity is 90% and temperature is 30° C, margins are about 1.3 and 1.1 dB for 20 and 30 GHz,

respectively. These margins moderately decrease for site locations above sea level. Note that for high-altitude locations, such as mountainous regions, hot and humid scenarios are unlikely; it is a very rare meteorological event if Denver, Colorado, experiences a 30° C temperature with relative humidity 90%, whereas the same event is not unusual for Austin, Texas.

3. Rain Attenuation

Rain attenuation is the most severe form of slant path atmospheric loss at 20/30 GHz frequencies. To predict the rain outage on Teledesic links, Crane's global model is used [2]. Crane's rain regions and their corresponding rain rate statistics are given in Table 1. This model divides the globe into twelve rain regions according to rain rate statistics and develops a procedure to predict the attenuation. This model was used to generate the global attenuation characteristics for the downlink and uplink of Teledesic's communications system, and the results are shown in the form of bar charts in Figures 3 and 4, respectively. For the downlink at 20 GHz frequency, the proposed communication system design assumes that the link has a rain margin of 9 dB. To see the sensitivity of link outage hours to the rain margin, we have taken 9 ± 3 dB, i.e., 6, 9, and 12 dB levels for the chart in Figure 3. Similarly for the uplink at 30 GHz frequency, the link design assumes a rain margin of 19 dB, and we have taken 19 ± 3 dB, i.e., 16, 19, and 22 dB levels for the chart in Figure 4. In both figures the path elevation angle is assumed to be 40°.

Table 1. Point Rain Rate Distribution Values (mm/h) Versus Hours per Year Rain Rate Exceeded

Hours per Year	Climate Regions											
	A	B1	B	B2	C	D1	D2	D3	E	F	G	H
0.44	14	22	29	35	41	50	65	81	118	34	121	178
0.88	10	16	20	24	28	36	49	63	98	23	94	147
1.75	7	11	14	16	18	24	35	48	78	15	72	119
4.38	4	6.4	8	9.5	11	15	22	32	52	8.3	47	87
8.77	2.5	4.2	5.2	6.1	7.2	9.8	15	22	35	5.2	32	64
17.5	1.5	2.8	3.4	4	4.8	6.4	9.5	15	21	3.1	22	44
43.8	0.7	1.5	1.9	2.3	2.7	3.6	5.2	7.8	11	1.4	12	23

Figure 3 shows a bar chart of the average number of service outage hours per year for the downlink at 20 GHz for all climatic regions without diversity in the global model. This chart shows that for the climatic regions A to D2 the average number of link outage hours per year is under 10 hours, and in some cases, as in regions A, B1, and B, it is in the vicinity of only 1 hour. For the regions D3

to F, the average number of link outage hours per year are larger than 10 hours, and in some cases, such as regions E, G, and H, the outage hours are substantially greater than 10.

Figure 4 shows a similar bar chart for the uplink frequency of 30 GHz. This chart is also drawn using the climatic zones in the global model. As in Figure 3, Figure 4 shows that for the regions A to D2, the average link outage hours per year are less than 10 hours, and in some regions (A, B1, and B) it is about 1 hour. For the regions D3 through H, the average outage hours per year are more than 10 hours, in some regions (E, G, and H) the outage is substantially greater than 10 hours.

Figure 5 shows measured rain attenuation statistics at Blacksburg, Virginia, resulting from Olympus measurements for a one-year period. From this figure, it can be seen that rain attenuation margins of 11 dB (20 GHz) and 21 dB (30 GHz) result in annual outage times of 9 and 10 hours for 20 and 30 GHz frequencies, respectively. Note that to account for gaseous and cloud attenuation, 2 dB is added to the margins of 9 dB and 19 dB at 20 GHz and 30 GHz, respectively. Blacksburg is in Region D2 of the global model, and the measurement year of Figure 5 received slightly more rainfall than the average year in Blacksburg [3].

4. Diversity

Teledesic is planning to use site diversity to improve link availability at gateway stations. The diversity principle is based on the fact that most high rain-rate cells are not very large and hence all the spatially diverse receiving stations provided in a diversity system may not suffer the worst rain attenuation at the same time. Obviously, more receiving stations as well as larger separating distances between the stations imply a better system performance, however, we will assume only two ground stations separated by a distance of 30 km.

The CCIR model for diversity rain attenuation prediction was used to predict the performance. The CCIR model computes the outage time percentage of the diversity system as a function of the outage time percentage of a single site. We have found good agreement between measured K_a-band diversity data reported in [4] and the CCIR prediction. The data had a diversity separation of 9 km and a path elevation angle of 26 degrees.

Figure 6 shows the percentage of time for two sites to exceed the desired level as a function of the percentage of time for a single site. The parameter is the diversity distance. Figures 7 and 8 show the average number of service outage hours per year for all climatic regions with diversity in the global model. Figure 7 is for the downlink at 20 GHz and at 6, 9, and 12 dB attenuation levels, and Figure 8 is for the uplink at 30 GHz frequency with 16, 19, and 22 dB attenuation

levels. The spatial diversity is assumed to be 30 km, and the ground station antenna elevation angle is assumed to be 40 degrees. These figures show that the link outage hours per year for both uplink and downlink are reduced compared with the earlier charts (Figures 3 and 4).

Figures 7 and 8 indicate that for large single-site outage times, i.e., larger than 10 hours per year, diversity improvement is small. However, this may be partly due to the inability of the CCIR model to accurately predict diversity improvement at large percentage values for Teledesic's links. It is possible that the CCIR diversity predictions for rain climate regions E, G, and H are pessimistic. This is an area that deserves further investigation.

5. Cloud Attenuation

The treatment of slant path cloud attenuation is not a simple task because it is difficult to separate cloud contribution from gaseous and rain contributions. For this reason there are no simple models for cloud attenuation that can be applied. Both analytical and experimental studies show that cloud attenuation is higher at 30 GHz than 20 GHz. Main contributing factors to signal attenuation are moisture content of the cloud and the slant path length through the cloud. Measurements have shown that at the 5% level, total zenith attenuation can vary from about 0.5 dB to more than 2 dB depending on the location of the site (from very dry to very wet regions) for 30 GHz signals [2]. These values, of course, include gaseous absorption.

Figures 9 and 10 show radiometrically produced statistics of total atmospheric attenuation at Denver, Colorado, for December 1987 and August 1988, respectively. At the 0.5% level, total attentions for 30 GHz are 0.75 and 2.1 dB, for December 1987 (dry) and August 1988 (humid), respectively.

In summary, it is difficult to separate clouds from other atmospheric contributors. For clear weather (no rain) conditions a 1-dB margin may be suggested for Teledesic's 20 and 30 GHz links. It is, however, difficult to associate reliable outage statistics to a 1-dB cloud margin. This is an area that deserves more research.

6. Fog Attenuation

The fog attenuation is very small and is not usually a factor in satellite link system design for frequencies below 100 GHz. Therefore, this attenuation could be ignored for Teledesic's 20- and 30-GHz links.

7. Sand and Dust Attenuation

Sand and dust can cause signal attenuation by scattering electromagnetic energy. Simulated measurements have shown that at 10 GHz and concentration of 10^{-5} g/m^3 the measured specific attenuation was less than 0.1 dB/km for sand and 0.4 dB/km for clay [2].

Sand and dust storms occur in certain regions of the world. The vertical extent of these storms is unknown, but it is unlikely that high concentrations would exceed 1 km. The slant path length in the case of Teledesic is expected to vary between zero and 2 km, generally resulting in a total additional attenuation due to sand less than 1 dB [2]. No measured satellite beacon data is available to confirm these results.

8. Depolarization

In radiowave propagation, depolarization refers to a change in the polarization state of the signal. This change is usually caused by wave propagation in the atmosphere. At frequencies below 10 GHz, the main cause of depolarization is the Faraday rotation: a rotation of the plane of polarization due to the interaction of radiowaves with electrons in the ionosphere. For frequencies above about 10 GHz, ionospheric effects can be ignored; however, for these frequencies hydrometeor-induced depolarization may pose a problem.

In satellite communications, rain and ice crystals are the prominent sources of signal depolarization. Radiowave propagation through rain and clouds with ice crystals can transfer a portion of the signal energy to an orthogonal polarization state. As will be demonstrated in this section, hydrometeor depolarization is often too small to affect the performance of single-polarized satellite communications links, however, it could have an adverse effect on dual-polarized systems.

Rain depolarization is usually associated with large rain attenuation, i.e., 15 dB, whereas ice depolarization can occur at relatively low attenuation levels, i.e., 2 dB. In general, depolarization due to rain is more frequent than due to ice. Ice depolarization is mainly observed in high-density, high-altitude clouds, such as clouds associated with thunderstorms. Low-latitude clouds are usually too warm to contain substantial amounts of ice. For predicting polarization effects at 20/30 GHz frequencies, the CCIR model can be used. In addition to the CCIR model, measured data from Olympus and other experiments are also available. A common measure of depolarization is a parameter known as cross-polarization discrimination (XPD). This parameter is defined as

$$XPD = \frac{\text{Power in the received co-pol signal}}{\text{Power in the received cross-pol signal}} \qquad (1)$$

For an ideal system, XPD is infinity.

The CCIR prediction model for depolarization due to rain has the following form:

$$XPD_{rain}(p) = a - b \log_{10}(A) \qquad (2)$$

where A is the total attenuation due to rain in dB, a and b are two empirical constants that depend on frequency, elevation angle, θ, and the polarization tilt angle with respect to the local horizon, τ. Note that dependence on p, time percentage, is implicit in A, a, and b. To also account for ice depolarization, the following model gives the total depolarization prediction

$$XPD_T(p) = [0.85 - 0.05 \log_{10}(p)]XPD_{rain}(p) \qquad (3)$$

Long-duration measurements of Olympus linearly polarized signals in Germany have yielded the following empirical relationship for the measured medians [5], where $\theta = 27°$ and $\tau = 21°$

$$XPD_{20} = 44.0 - 21.8 \log_{10}(A_{20}) \quad \text{(dB)}$$
$$XPD_{30} = 46.5 - 21.4 \log_{10}(A_{30}) \quad \text{(dB)} \qquad (4)$$

Because the above models are obtained from one year of measurement data in Germany, its applicability to other climatic and geographic zones should be made with caution.

To demonstrate the effect of depolarization, Figure 11 shows the cumulative distribution of XPD for Darmstadt, Germany, for $\theta = 27°$ and $\tau = 21°$ [6]. This site was selected because multiyear Olympus measurements exist at this site. Figure 11 also shows the measured values. For this particular data set, the CCIR model underestimates the effect of depolarization.

Figure 12 shows the cumulative distribution of predicted XPD for Blacksburg, Virginia, assuming circular polarization. Measured Olympus rain attenuation data at 14° elevation angle [7] were scaled to 40° and then used to obtain Figure 12. Note that there are no XPD measured data at Blacksburg.

Olympus 20 and 30 GHz data are also available from the British Telecom site near Ipswich, England [8]. Although these measurements were made at a low elevation angle of 27.5°, the measured values of XPD are high at the percentage values of interest to Teledesic as shown in Figure 13. For example, at a percentage value of 0.1, XPD is higher than 20 dB for both frequencies.

Considering the predicted and measured data provided in this section, the following conclusion can be reached: At a percentage level of 0.1, XPD measurements, as well as predictions, are higher than 20 dB for both frequencies. This value of XPD provides a comfortable margin for Teledesic links. Therefore, assuming that Teledesic does not intend to use dual polarization transmissions, the effect of depolarization can safely be ignored. However, if Teledesic plans in the future to employ dual polarization transmissions to a cell as a means of frequency reuse, depolarization is likely to play a role. In summary, depolarization does not seem to be an issue for the present design of the Teledesic network.

9. Scintillation Effects

Tropospheric scintillation implies rapid fluctuation of signals caused by electromagnetic wave scattering and diffraction due to small scale turbulent refractive index inhomogeneities in the troposphere. Low-latitude tropospheric layers and clouds (especially fair weather cumuli) are considered the prime sources of K-band scintillation. The estimation of scintillation intensity in satellite links is obtained via a model that attributes scintillation to a thin turbulent layer about 1 km above the Earth station [1]. Scintillation intensity is a function of humidity, temperature, path elevation angle, and frequency. The size of the Earth station antenna also has a weak-to-moderate effect on the observed intensity of scintillation. The relationship is of inverse type with larger aperture sizes producing less scintillation fading than the smaller ones. The existing CCIR model has been frequently tested at Ku-band frequencies with good results. The available K_a-band database, however, is small compared to the Ku-band, and therefore, only a limited number of tests have been performed on the CCIR model at 20/30 GHz. The few examinations of the CCIR model at K_a-band have been positive so far.

Because Blacksburg, Virginia, is one of the rare sites in the U.S. with K_a-band scintillation data, we have chosen this site to produce Figures 14 and 15. These figures show cumulative fade statistics due to scintillation estimated for Teledesic links using the CCIR method. K_a-band scintillation data collected at Blacksburg have shown good-to-moderate agreement with the CCIR model for a 14° elevation angle [9]. These data were collected during the Olympus campaign at Blacksburg. Figure 14 shows the average yearly effect, whereas, Figure 15 is based on a one-month period in late spring when scintillation

intensity is high because of high humidity and warm weather conditions. These figures indicate that for climate regions exemplified by Virginia, USA, 1 dB of margin is sufficient to protect the Teledesic link from scintillation fading for more than 99.99% of the time. No spatial diversity is assumed for combating scintillation.

Figure 16 shows the cumulative fade statistics of scintillation for average conditions at Austin, Texas. Austin has warm and humid weather -- a high scintillation region. The worst case situation in Austin is shown in Figure 17. According to this figure, in rare occasions, fades deeper than 1-dB can be observed in Austin.

10. Propagation Margin Summaries

Recommended **gaseous attenuation** margins in dB are given in Table 2.

Table 2. Gaseous Attenuation in dB

Region	20 GHz		30 GHz	
	No Rain	Rain	No Rain	Rain
Dry	0.3		0.3	
Warm & Humid	1.3	1.8	1.1	1.5

The global model predicts rain attenuation with respect to clear air, whereas the CCIR model predicts total attenuation (cloud and atmospheric attenuations are partially included). Hence when using the global model, gaseous attenuation during rain should be obtained from Table 2 minus 0.3 dB (e.g., 1.5 dB and 1.2 dB for 20 GHz and 30 GHz frequencies, respectively). For the CCIR model, there is no need to add gaseous attenuation to rain attenuation, because gaseous attenuation is already included in the rain attenuation model.

Average outage hours per year due to **rain attenuation** assuming margins of 9 and 19 dB for 20 and 30 GHz frequencies, respectively, are given in Table 3. This table contains values with and without **space diversity**.

Table 3. Rain Attenuation

Region	A	B1	B	B2	C	D1	D2	D3	E	F	G	H
Hours	0.2	0.8	0.5	1.0	4.0	3.5	6.5	15	31	3.0	50	89
Hours with Diversity	0.0	0.0	0.0	0.0	0.2	0.2	0.7	2.5	5.5	0.1	18	41

The recommended **cloud attenuation** (above gaseous attenuation) margin is 1 dB.

Fog attenuation can be ignored.

Sand and **dust attenuation** can generally be ignored for most regions of the world. In regions with high probability of heavy sand or dust storms, a 1-dB margin is recommended.

Depolarization loss can be ignored for single-polarization transmissions to the same location.

For **scintillation fading** a margin of 1 dB is recommend for hot and humid locations (high scintillation conditions).

11. International Telecommunications Union

The International Telecommunications Union is an intergovernmental organization, and any sovereign state may become a member of this union. Their governments (in most cases represented by their telecommunications administrations) are constitutional members with special obligations, but also enjoy special rights, e.g., the right to vote. Other organizations such as network and service providers, manufacturers, scientific, and other international organizations (e.g., Teledesic), may be admitted through their national administrations to certain ITU activities, such as standardization, but enjoy a lower legal status with no right to vote.

Three main functions that are carried out globally by ITU are as follows:

1. Standardization of telecommunications.
2. Development of telecommunications.
3. Regulation of telecommunications (mainly for radio communications).

The standards developed by ITU are called *recommendations*. This term implies that they constitute nonbinding, voluntary agreements in contrast to the term *standard*, which is often used for mandatory, binding norms.

Consistent with its international nature, Teledesic can and should play a strong role in the first two functions of ITU. Participation in ITU functions will provide visibility in the international scene as well as pave the road for receiving regulatory support from future Teledesic client states. Because of the obvious benefits to its objectives, ITU welcomes and encourages the participation of international network and service providers in its activities.

Recommendations are developed in the Study Groups of the Radio Communications and Telecommunications sectors. These sectors are also known as ITU-R and ITU-T[1], respectively. Each study group deals with a specific area in radio communications or telecommunications. Study group members are *delegates* sent by their administrations. Other organizations may also participate by sending their experts as *participants* if their organization has been admitted by their national administration to the activities of ITU-R or ITU-T.

Study groups of interest to Teledesic are ITU-R Study Groups 4 and 8, dealing with the areas of fixed and mobile satellite communications, respectively. Teledesic's specific approach in treating propagation problems should also be brought to the attention of Study Group 5 of ITU-R since microwave propagation is in the domain of this study group. The contact with Study Group 5 can be made either directly or through Study Groups 4 and 8.

12. References

1. *1992 CCIR Recommendations,* RPN Series, Propagation in Non-Ionized Media, ITU, Geneva, 1992.

2. L. Ippolito, *Propagation Effects Handbook for Satellite Systems Design,* NASA Reference Publication 1082 (04), NASA, Washington, DC, 1989.

3. J. Laster and W. Stutzman, *Attenuation Scaling by frequency in the Ku/K_a-Band Using the Olympus Satellite*, SATCOM Report No 93-16, Virginia Tech, Sept. 1993.

4. K. Lin and C. Levis, "Site Diversity for Satellite Earth Terminals and Measurements at 28 GHz," *Proc. of the IEEE*, Vol 81, No 6, June 1993, pp. 897-904.

5. R. Jakoby and F. Rücker, "Three Years of Crosspolar Measurements at 12.5, 20, and 30 GHz with the Olympus Satellite," *Proc. Olympus Utilization Conf.*, Sevilla, Spain, Apr. 20 - 22, 1993, pp. 567 - 672.

6. F. Dintelman, G. Ortgies, F. Rücker, and R. Jakoby, "Results from 12- to 30-GHz German Propagation Experiments Carried Out with Radiometers and the Olympus Satellite," *Proc. IEEE*, Vol. 81, No. 6, June 1993, pp. 876 - 884.

7. W. Stutzman, et al., "Statistical Results from the Virginia Tech Propagation Experiment Using the Olympus 12, 20 and 30 GHz Satellite Beacons," *Proc.*

[1] In December 1992, an ITU Plenipotentiary Conference introduced three new sectors: *Radio Communications* (formerly CCIR and IFRB), *Telecommunications Standardization* (formerly CCITT), and a new *Development Sector.*

Seventeenth NASA Propagation Experimenters Meeting (NAPEX XVII), JPL Publication 93-21, JPL, Pasadena, CA, Aug. 1, 1993, pp. 33 - 45,

8. R. Howell, J. Harris, and M. Mehler, "Satellite Crosspolar Measurements at BT Laboratories," *BT Technology Journal*, Vol. 10, No. 4, Oct. 1992, pp. 52 - 67.

9. T. Pratt and F. Haidara, "Results from a Study of Scintillation Behavior at 12, 20, and 30 GHz Using the Results from the Virginia Tech Olympus Receivers," *Proc. Seventeenth NASA Propagation Experiments Meeting (NAPEX XVII)*, JPL Pub 93-21, JPL, Pasadena, CA, Aug. 1, 1993, pp. 47-58.

Acknowledgment

The research described in this publication was carried out by the Jet Propulsion Laboratory, California Institute of Technology, and was sponsored by Teledesic corporation.

GASEOUS ABSORPTION

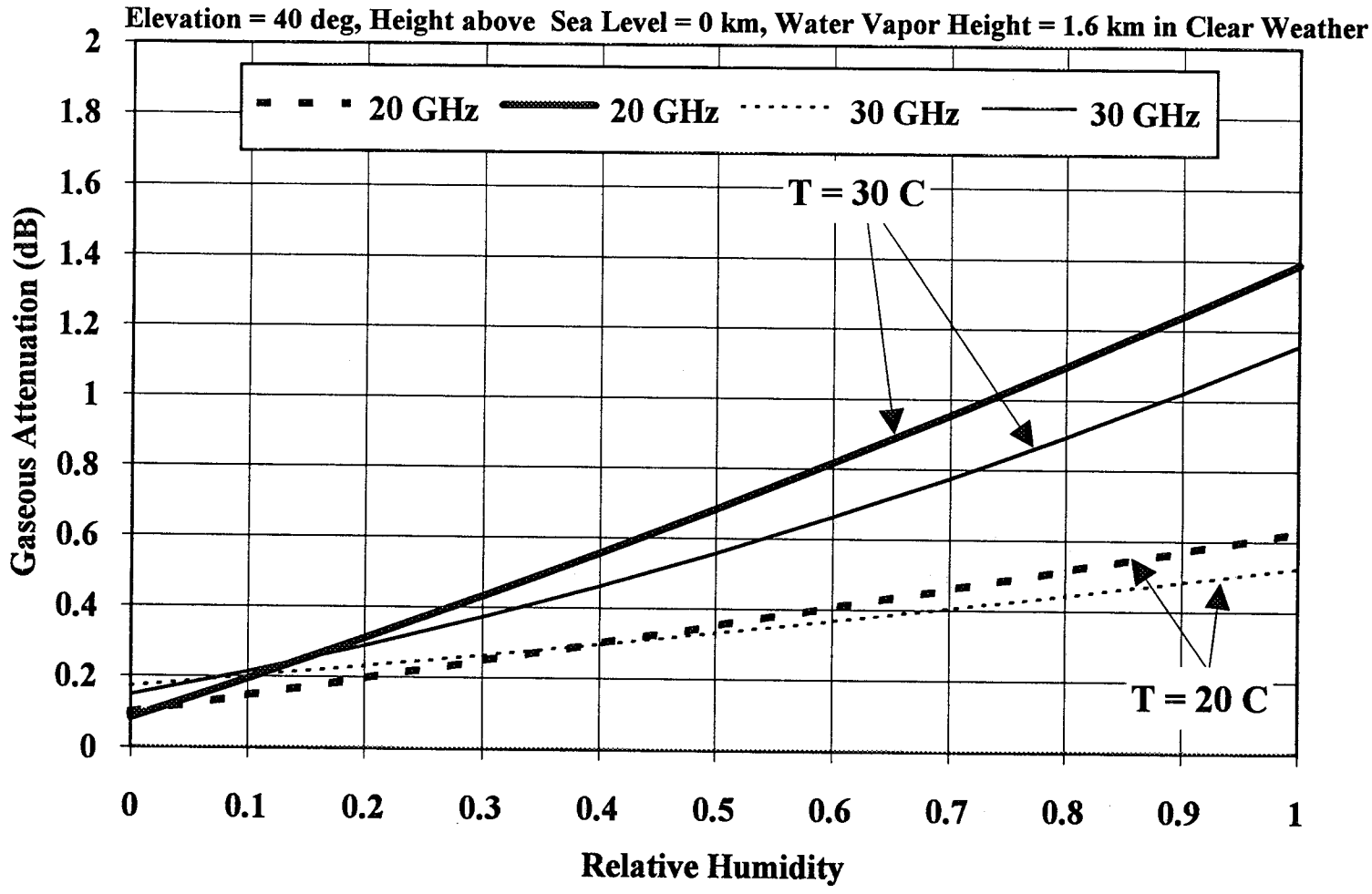

Figure 1: Gaseous Attenuation due to Oxygen and Water Vapor in Clear Weather.

GASEOUS ABSORPTION

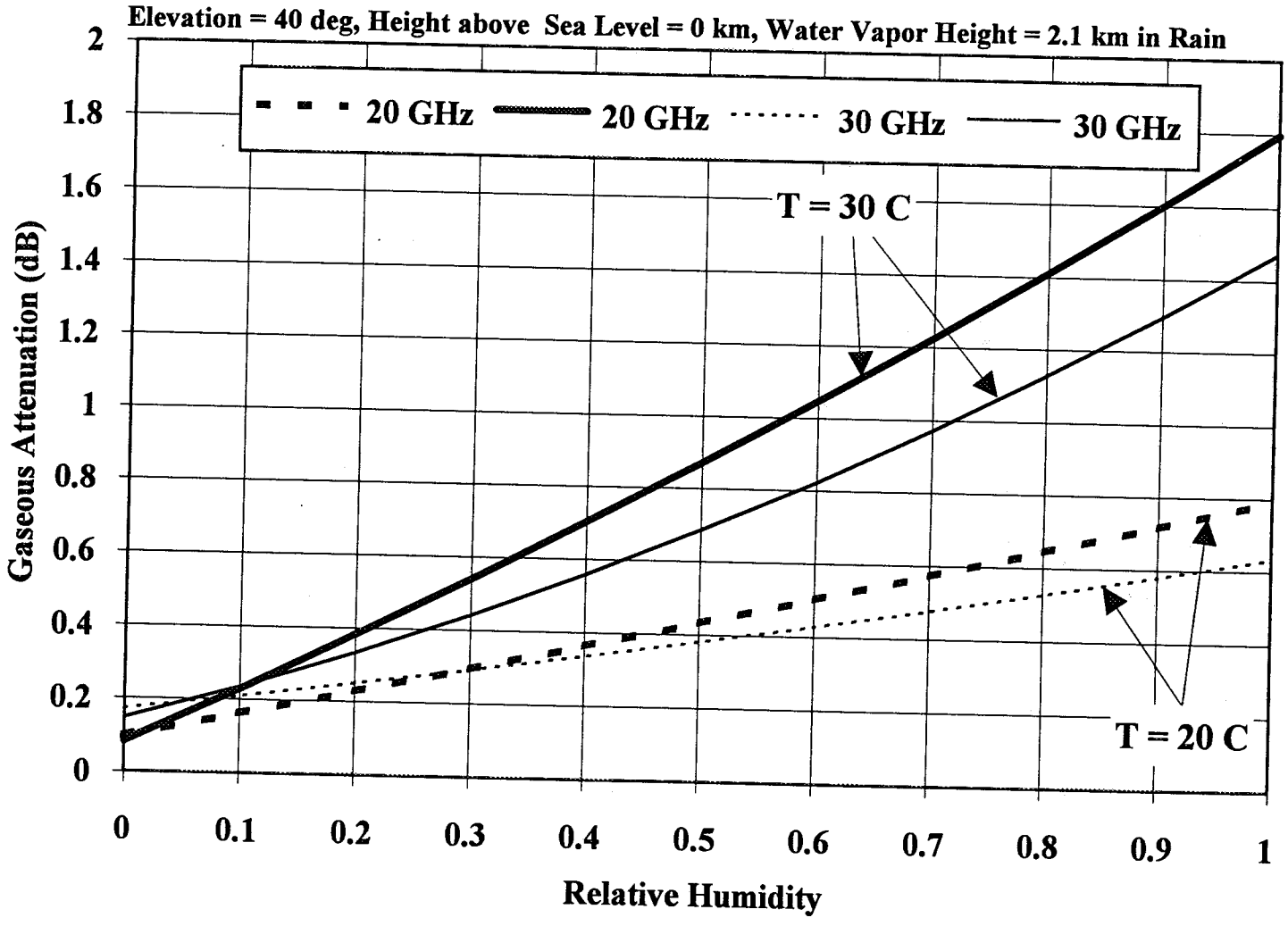

Figure 2: Gaseous Attenuation due to Oxygen and Water Vapor in Rain.

RAIN ATTENUATION

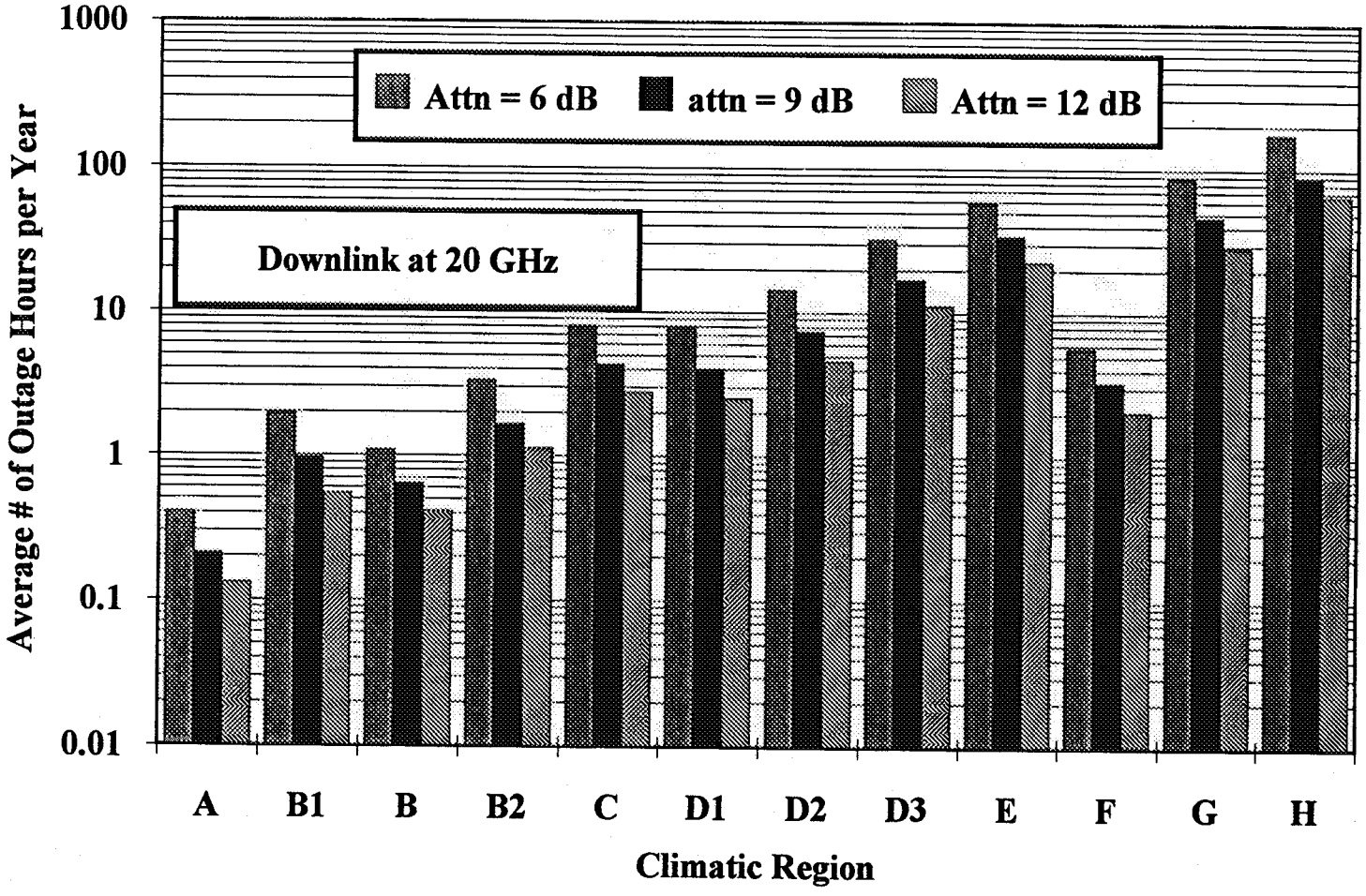

Figure 3: Average Number of Link Outage Hours per Year with No Spatial Diversity.

RAIN ATTENUATION

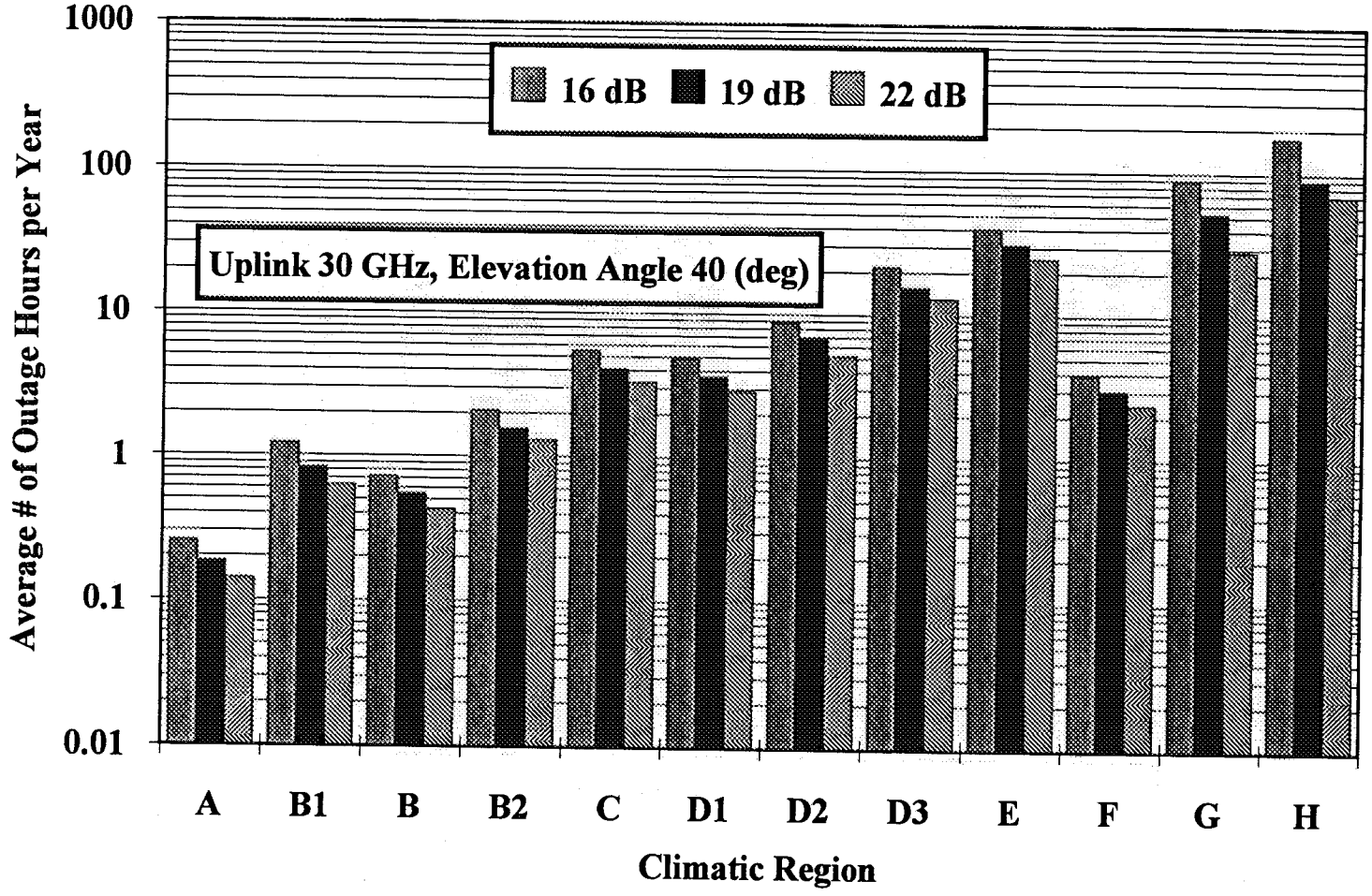

Figure 4: Uplink Average Number of Link Outage Hours per Year with No Spatial Diversity.

RAIN ATTENUATION

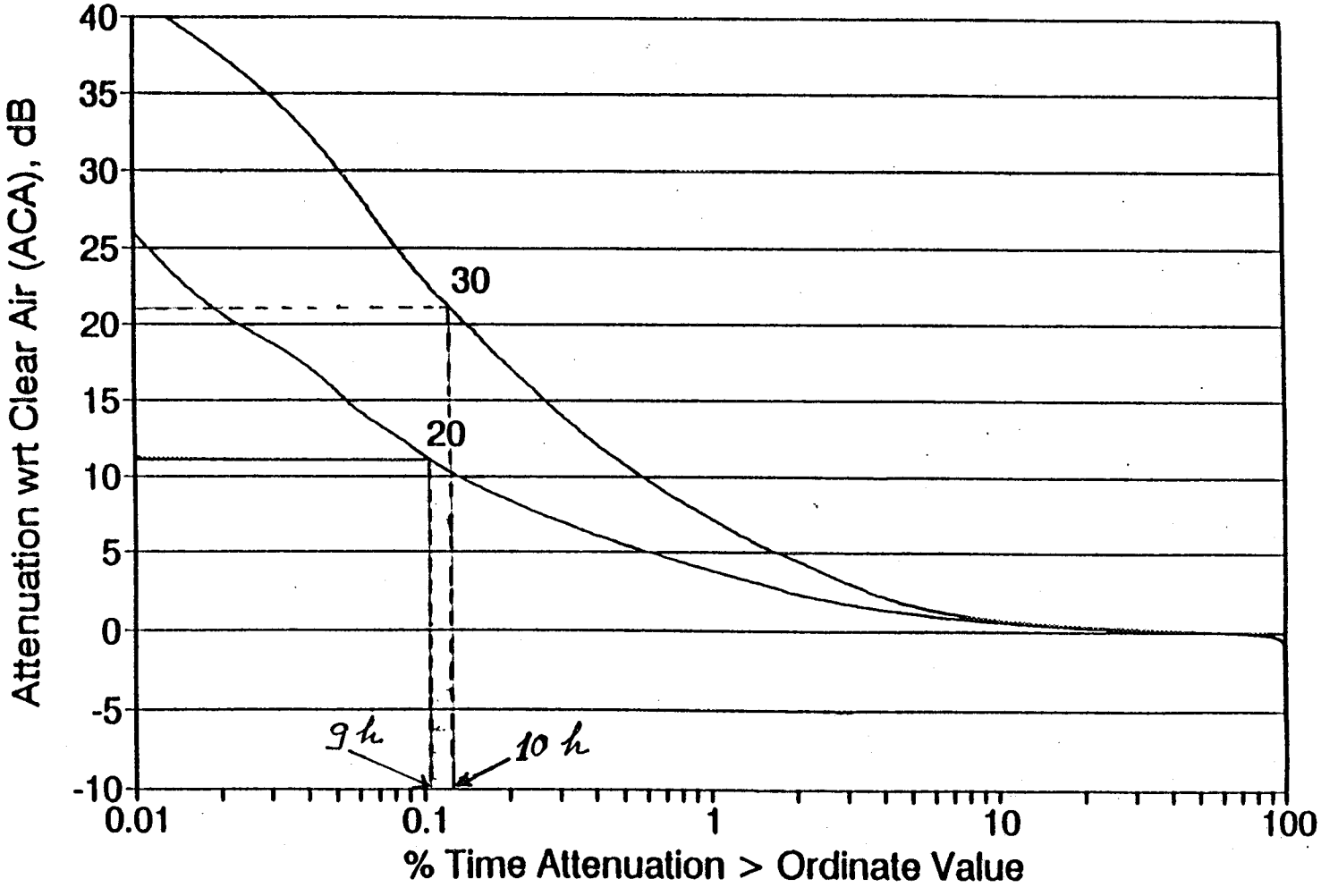

* Common Time Base

Figure 5: Attenuation with Respect to Clear Air at 20 & 30 GHz (91/92)-Blacksburg, Virginia.

CCIR DIVERSITY MODEL

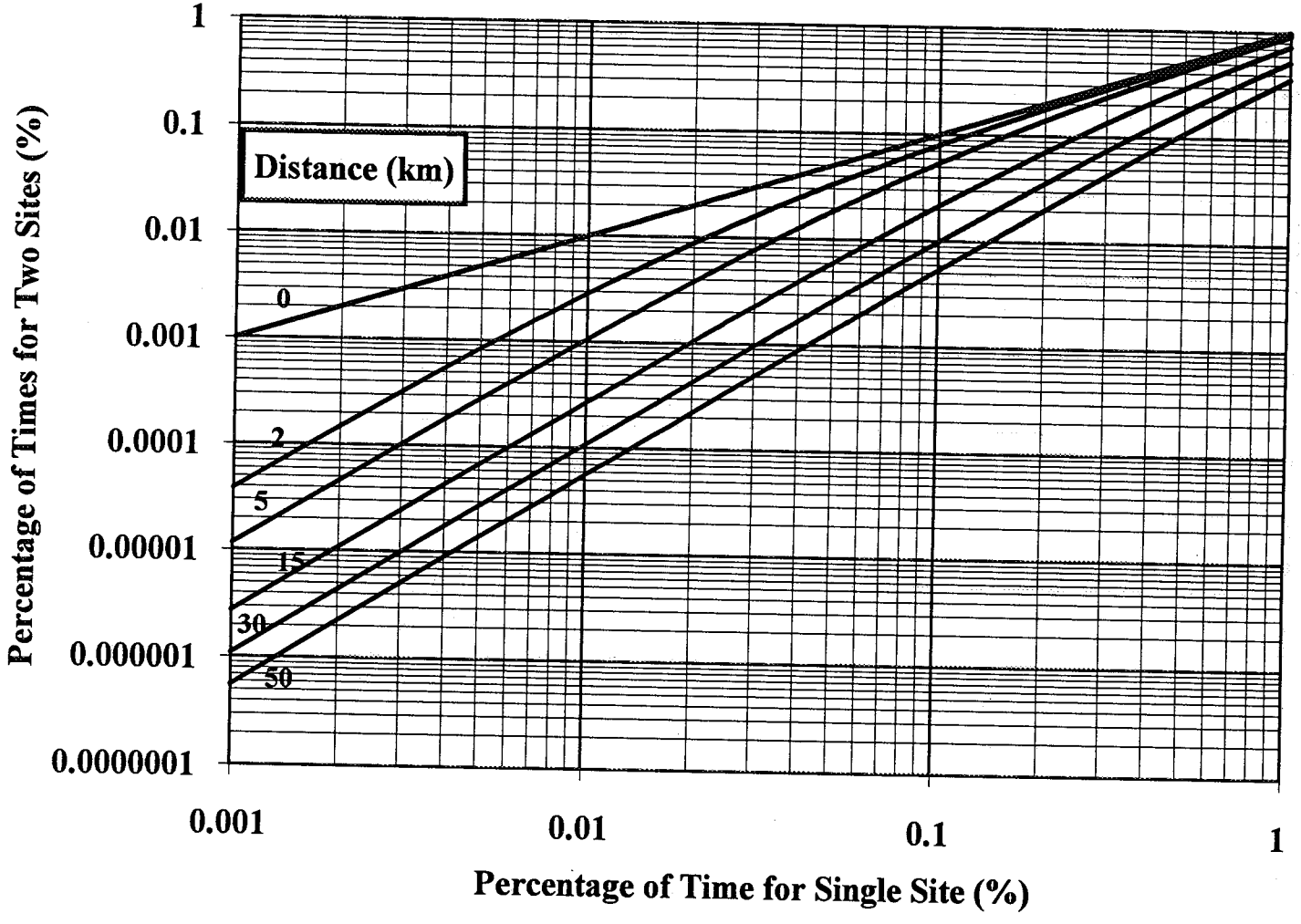

Figure 6: Diversity Improvement with Two Sites.

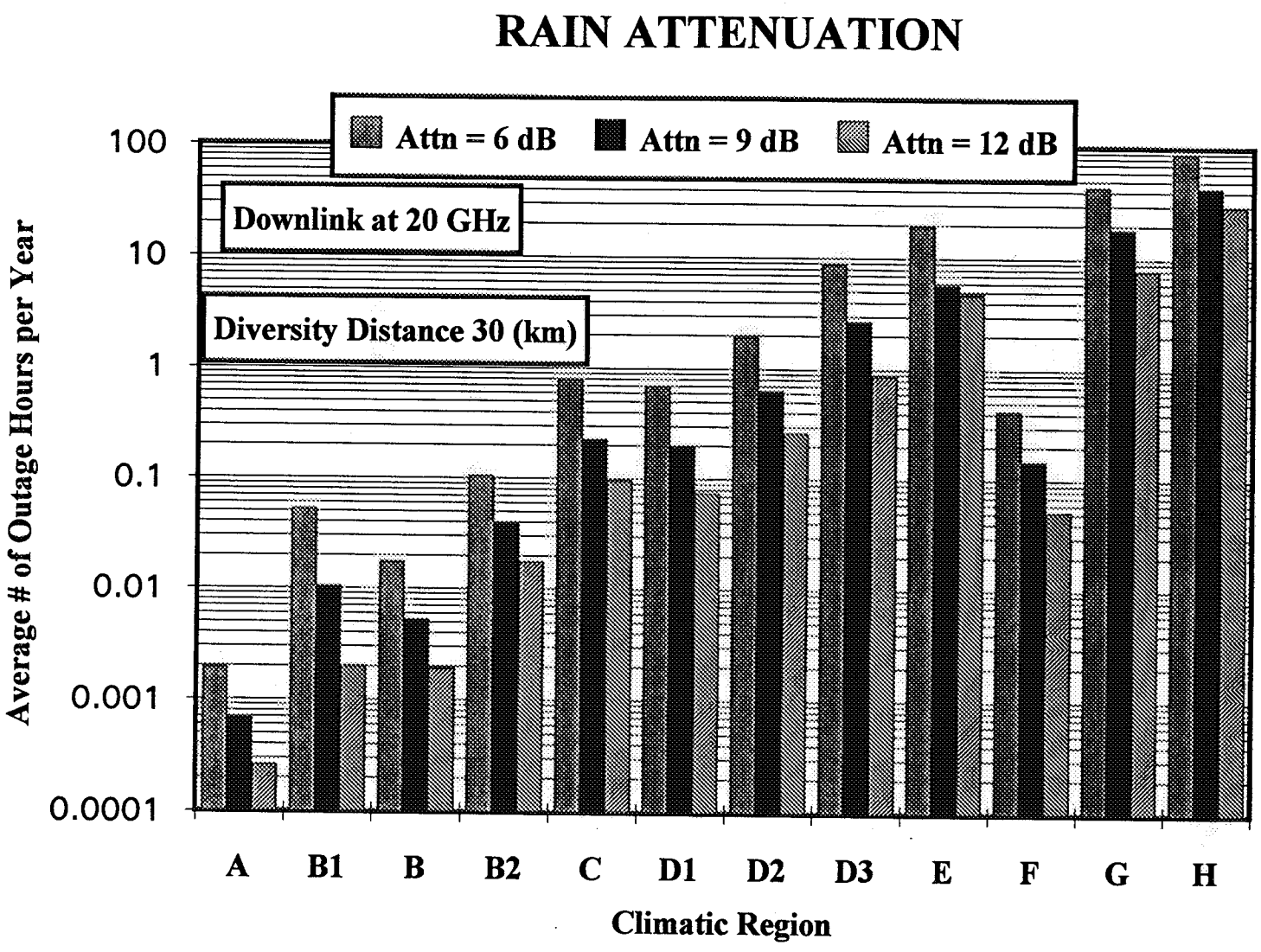

Figure 7: Average Number of Link Outage Hours per Year with Spatial Diversity.

RAIN ATTENUATION

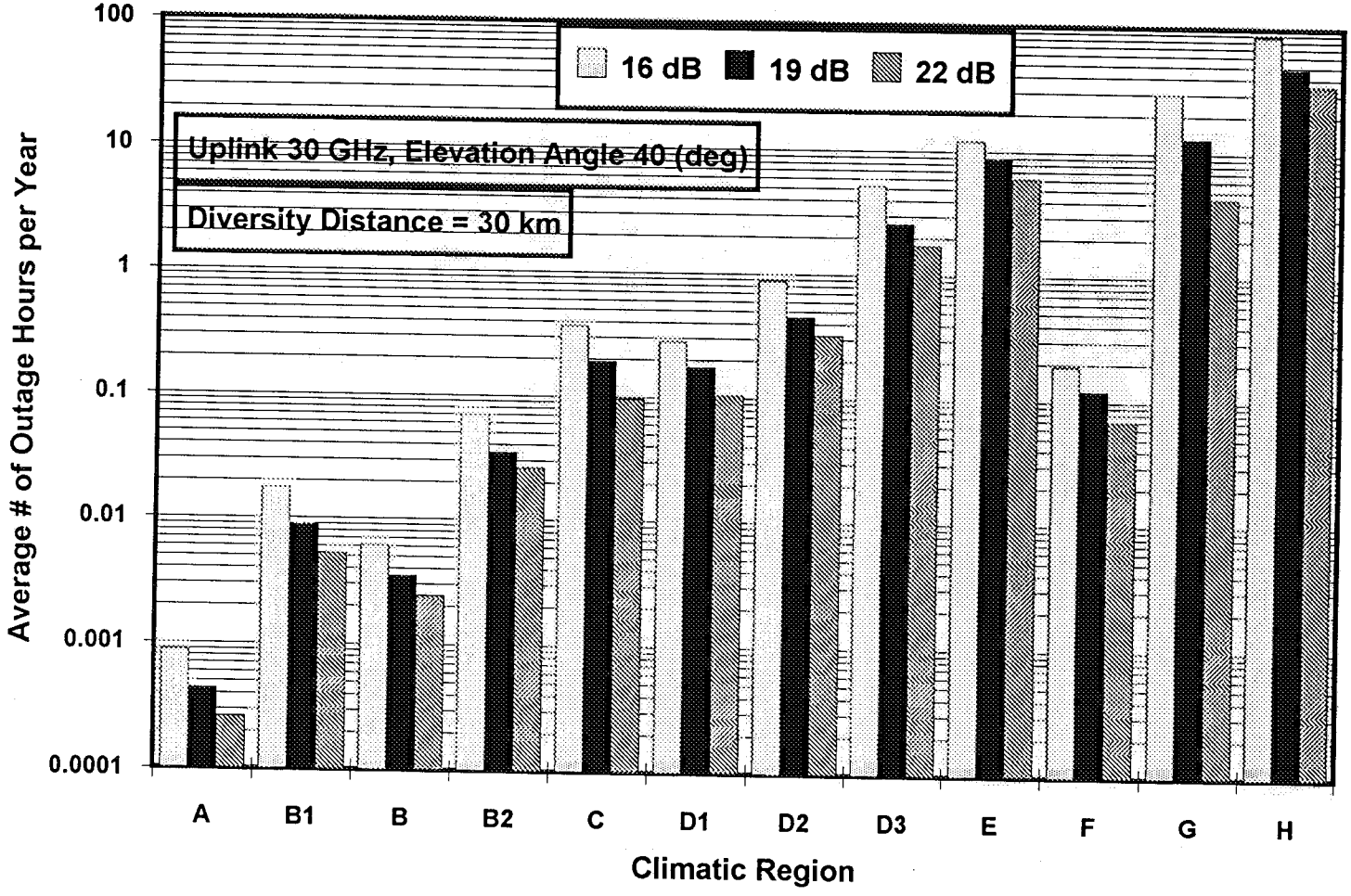

Figure 8: Average Number of Link Outage Hours per Year with Spatial Diversity

ZENITH ATTENUATION

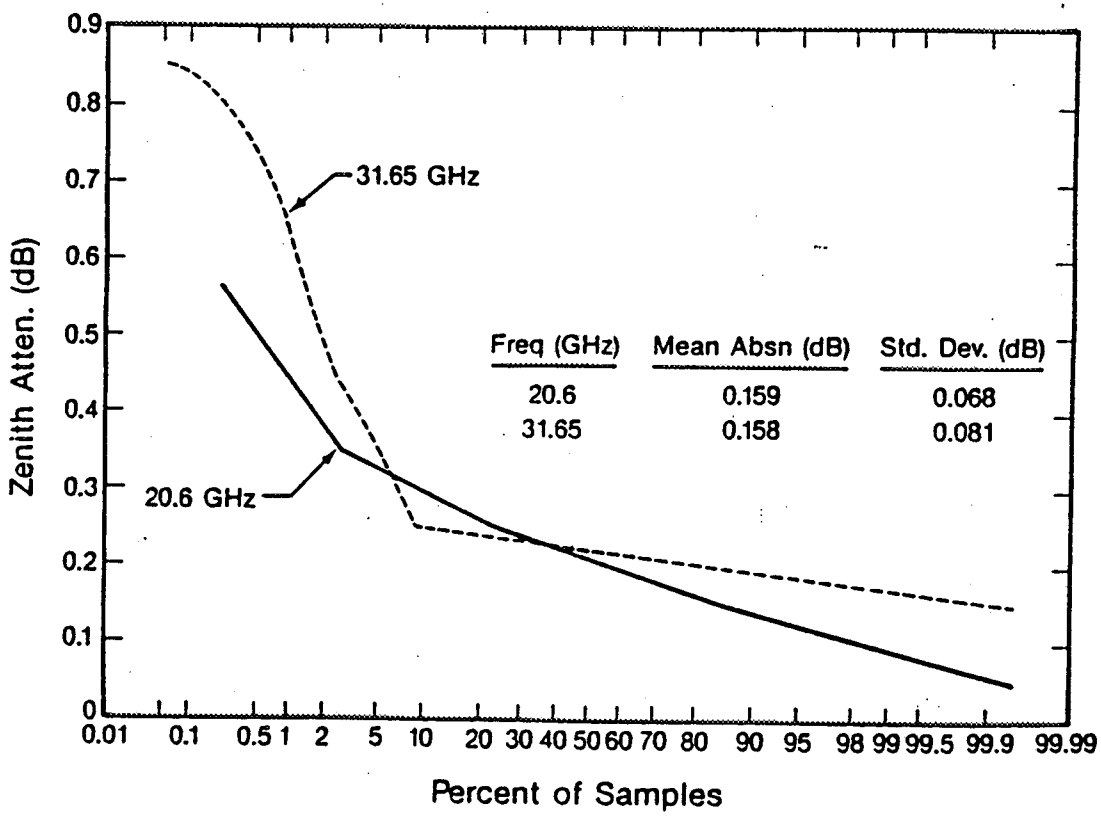

Figure 9: Cumulative Distribution of Zenith Attenuation Measured by a Three-Channel Radiometer at Denver, Colorado, December 1987. Data Consist of 14181 2-min Averages.

ZENITH ATTENUATION

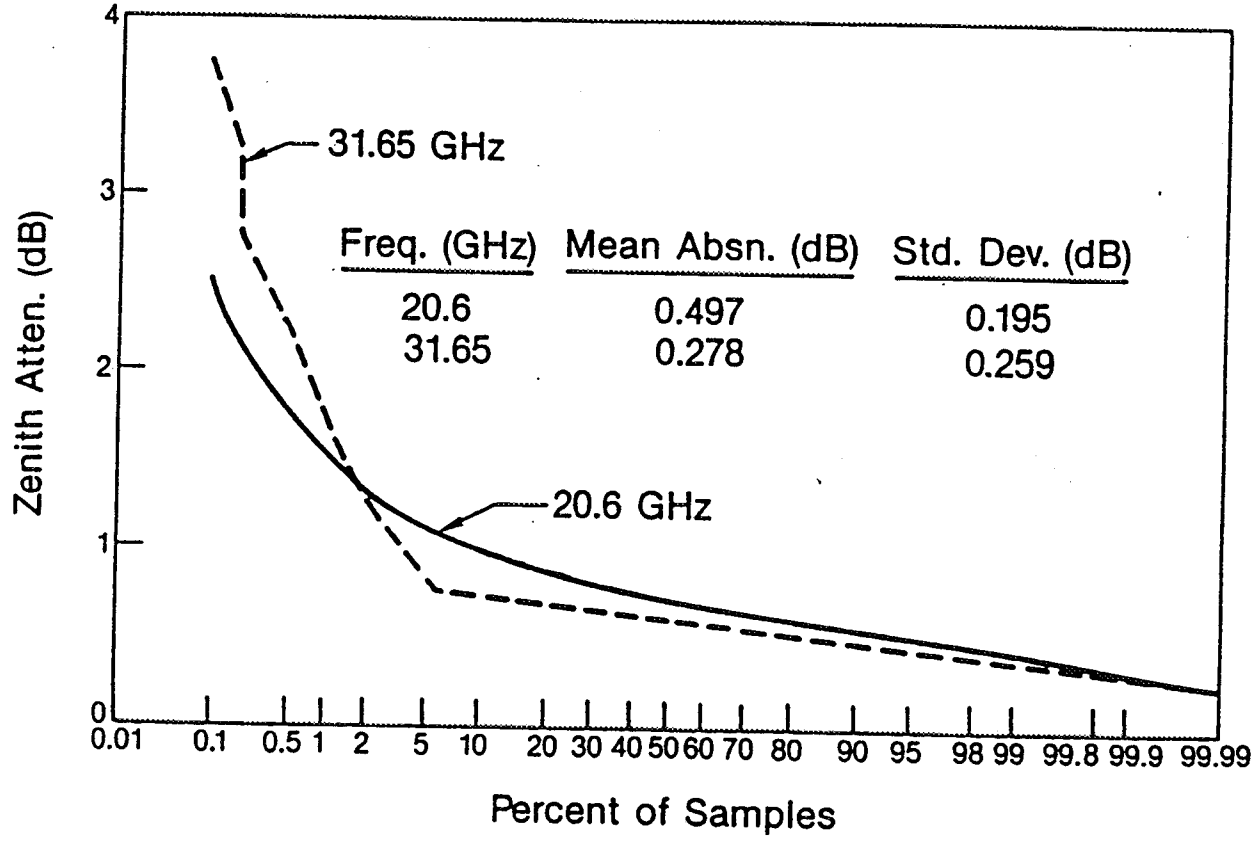

Figure 10: Cumulative Distribution of Zenith Attenuation Measured by a Three-Channel Radiometer at Denver, Colorado, August 1988. Data Consist of 17792 2-min Averages.

DEPOLARIZATION

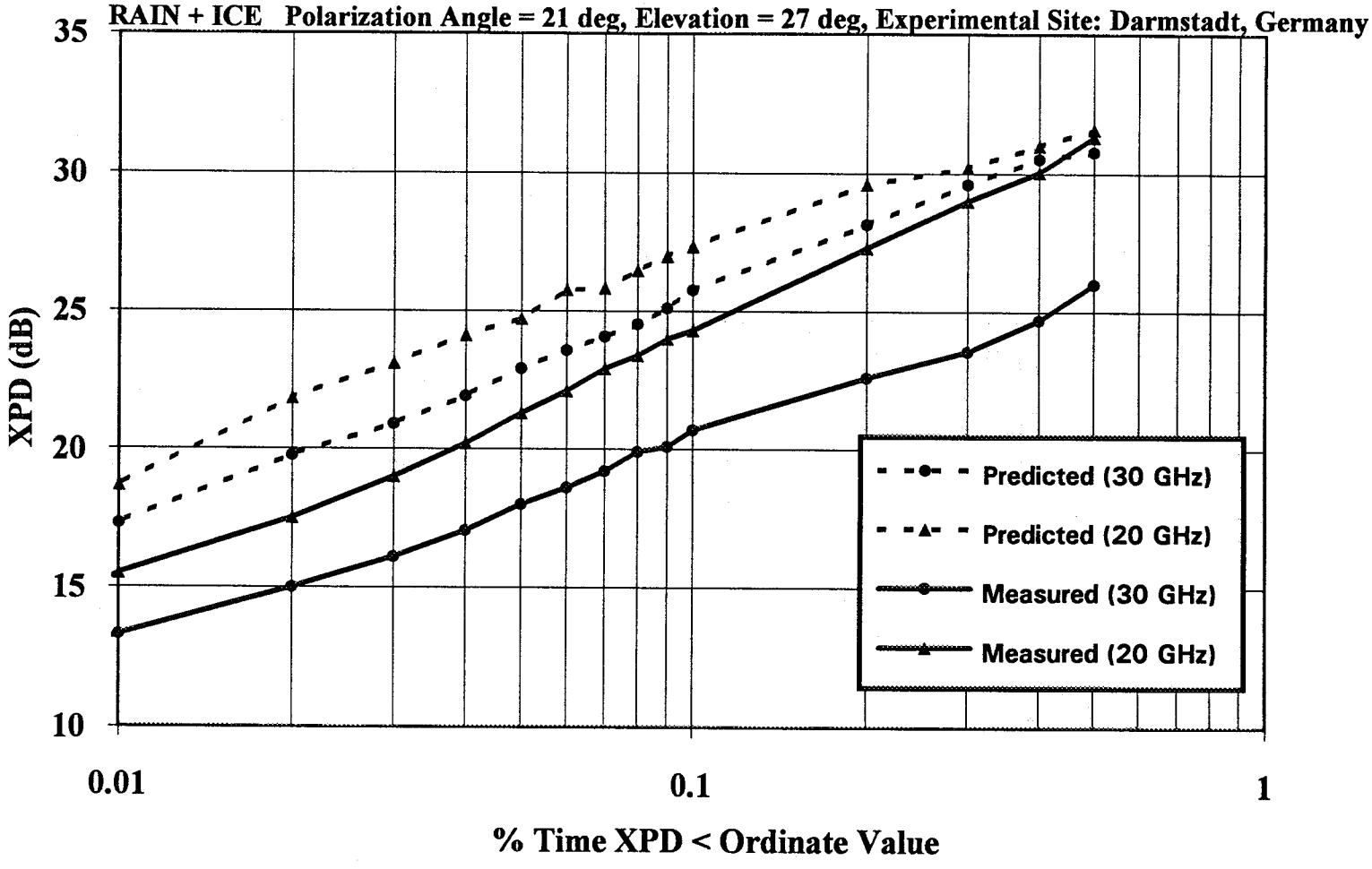

Figure 11: Cumulative Distributions of Measured XPD and CCIR Predictions Based on Measured Attenuation at 20 and 30 GHz.

DEPOLARIZATION

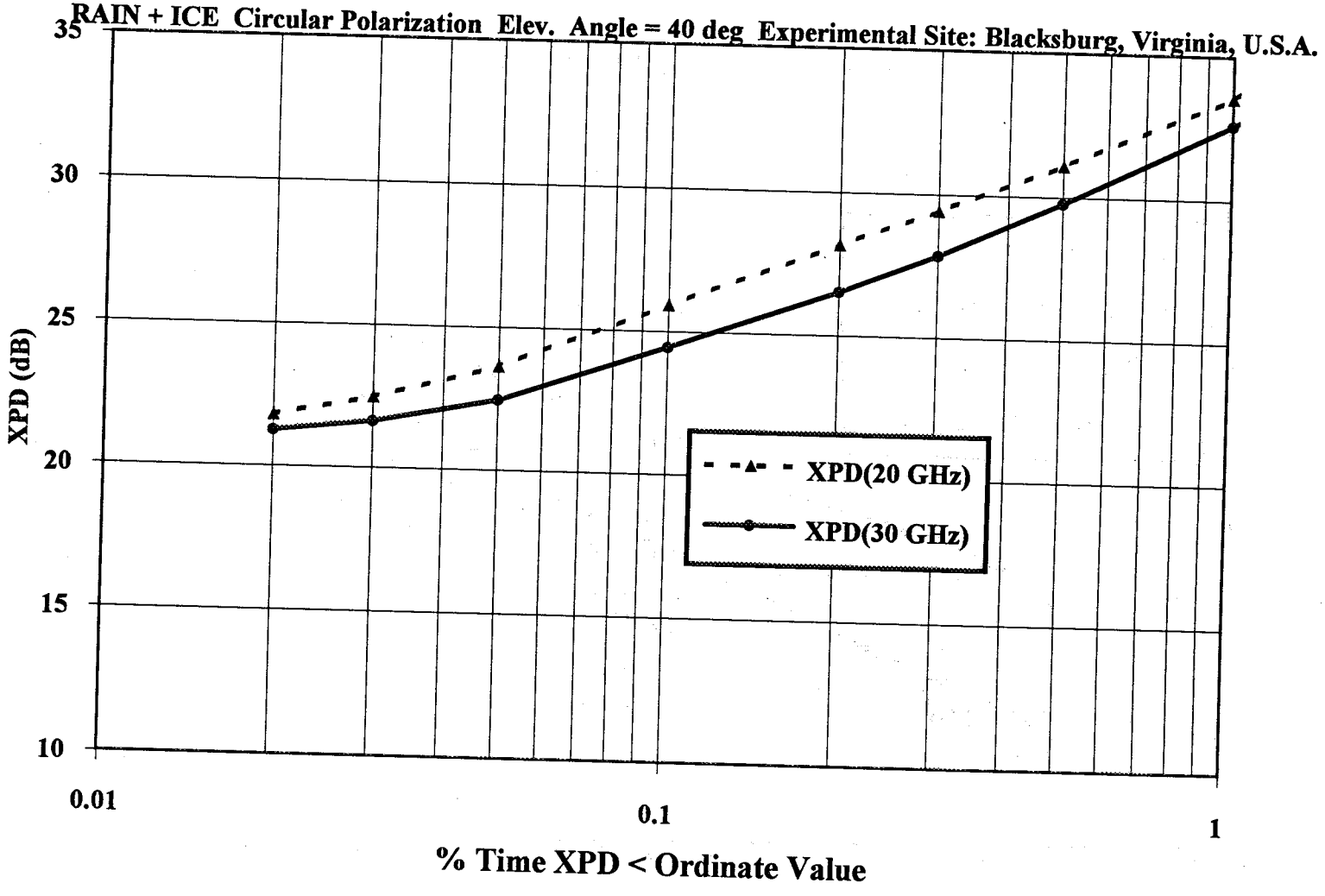

Figure 12: Cumulative Distribution of XPD for Blacksburg, Virginia.

DEPOLARIZATION

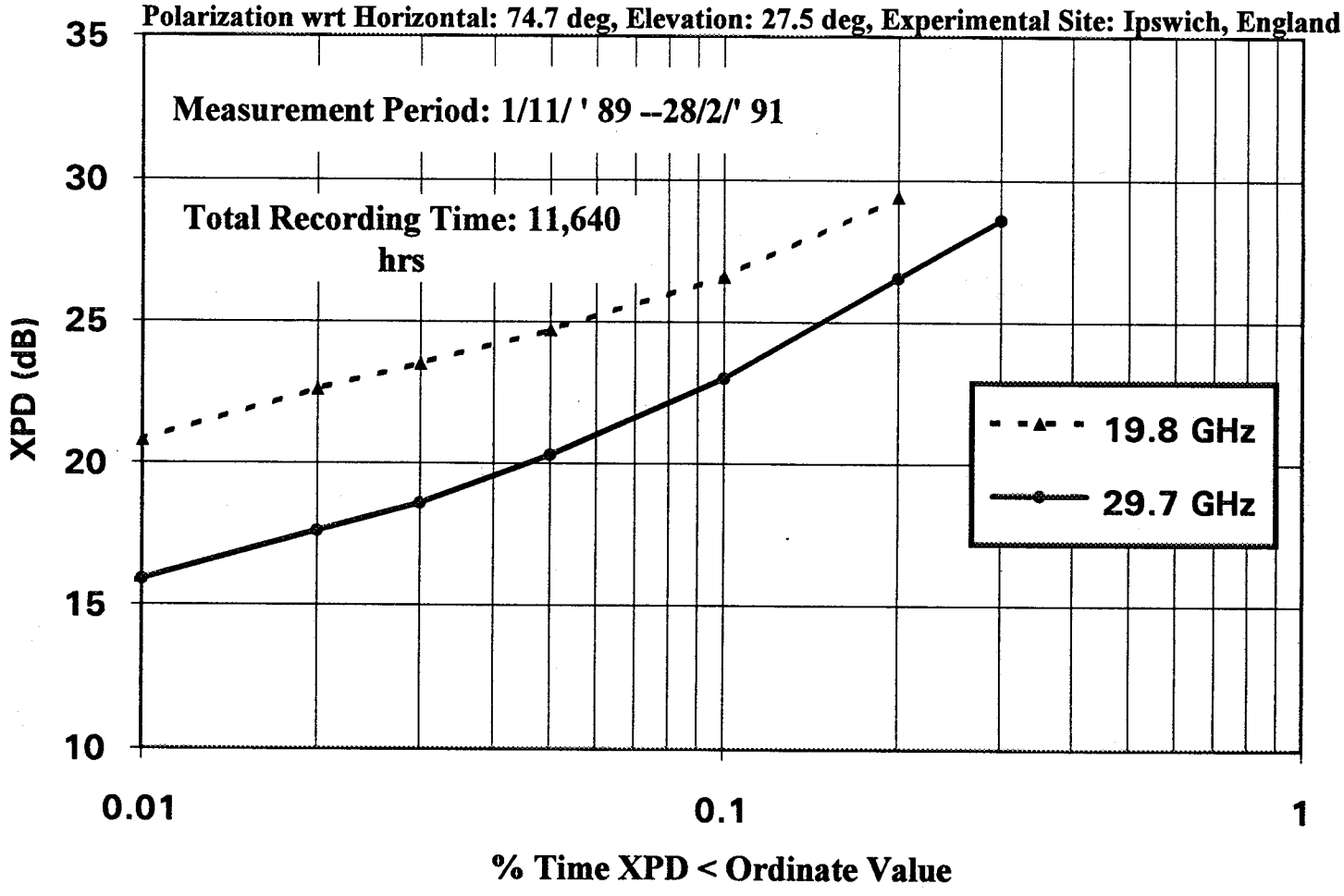

Figure 13: Crosspolar Discrimination Measured Data from OLYMPUS at 19.8 and 29.7 GHz.

SCINTILLATION

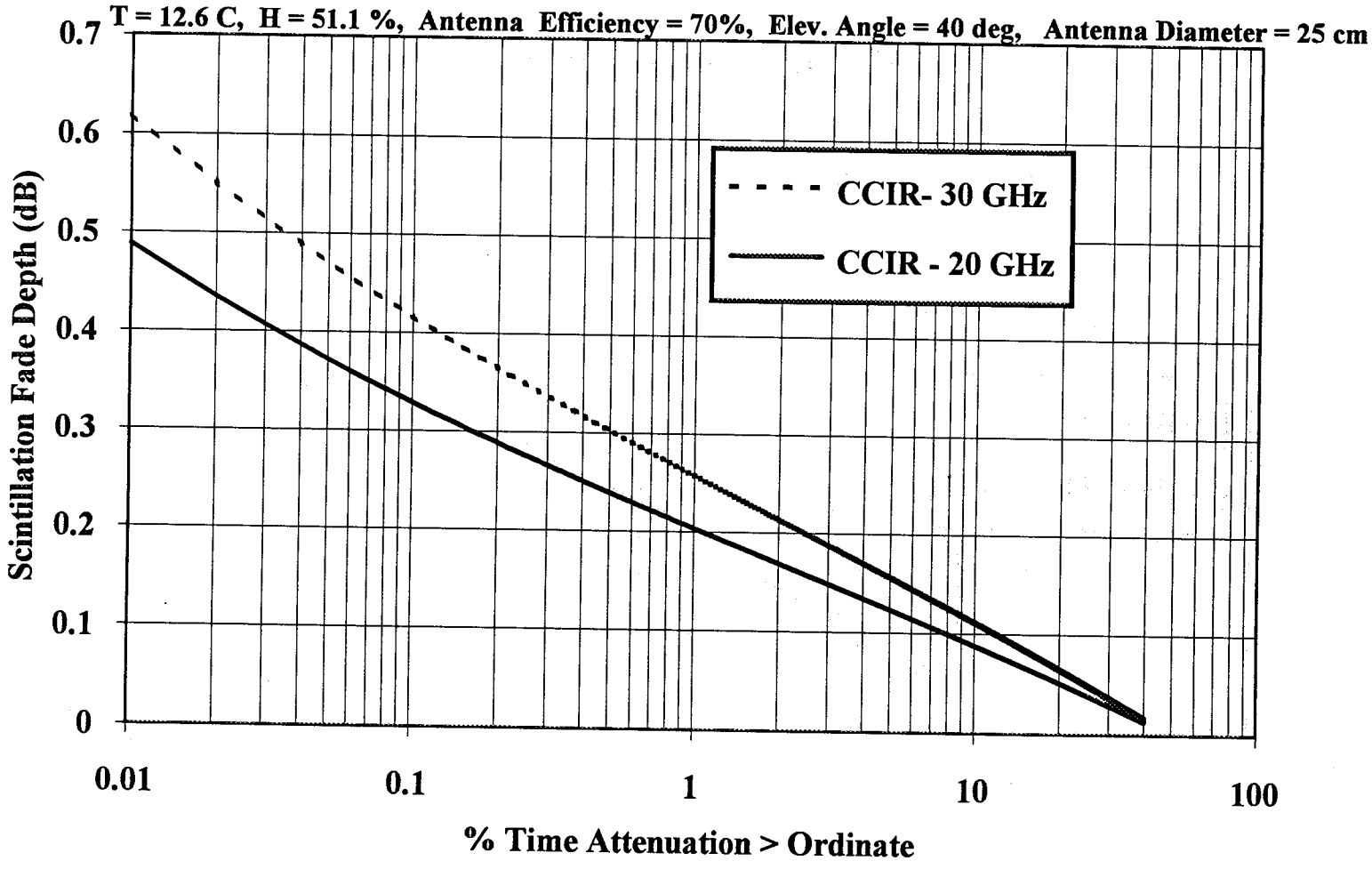

Figure 14: Cumulative Scintillation Fade Distribution, Blacksburg, VA, Average Conditions.

SCINTILLATION

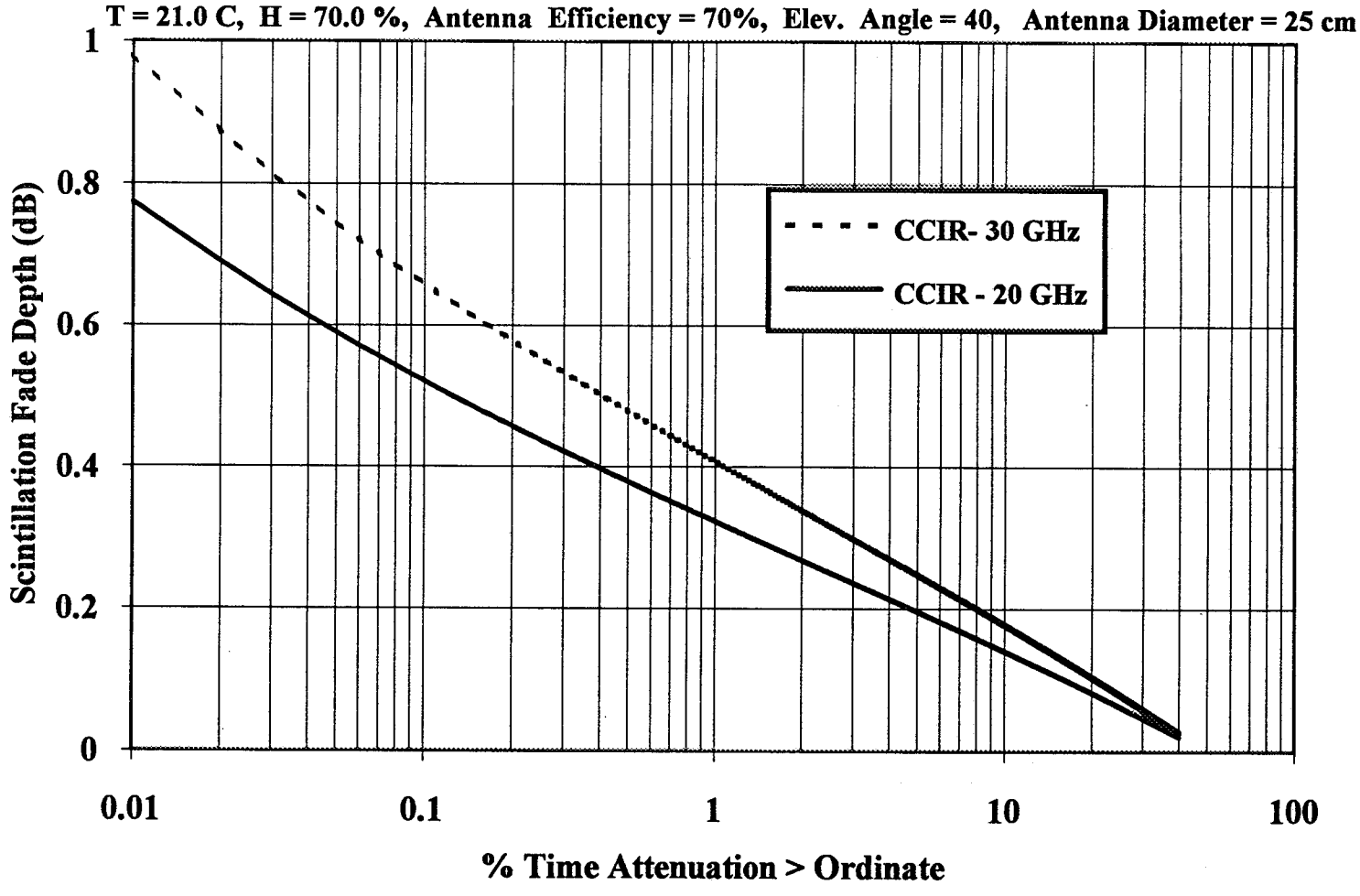

Figure 15: Cumulative Scintillation Fade Distribution, Blacksburg, VA, Spring/Summer Conditions.

SCINTILLATION

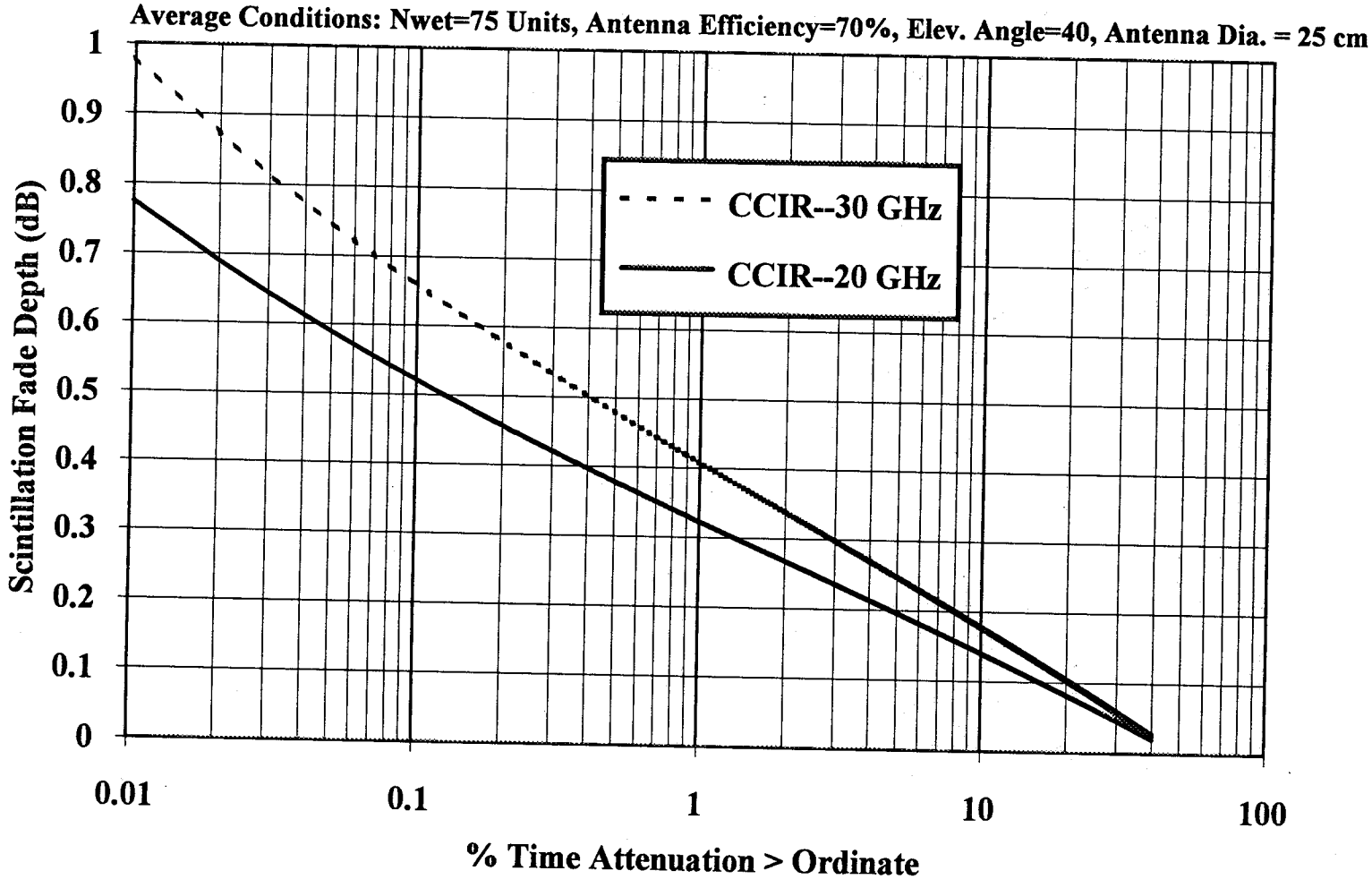

Figure 16: Cumulative Scintillation Fade Distribution, Austin, TX, Average Conditions.

SCINTILLATION

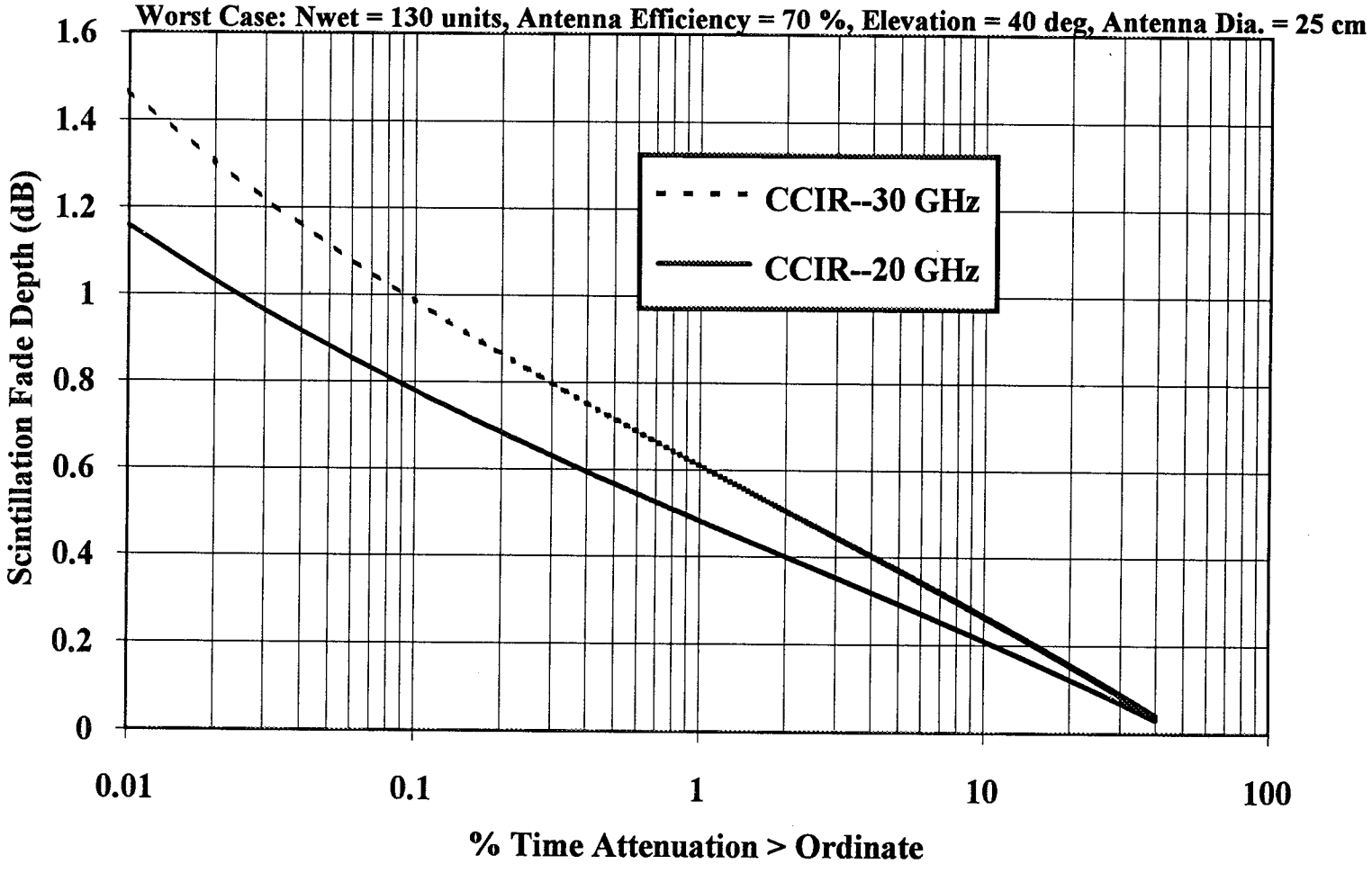

Figure 17: Cumulative Scintillation Fade Distribution for Worst Case Conditions at Austin, Texas.